# Structure–Property Relationships of Thermoplastic Polyurethane Elastomers Based on Polycarbonate Diols

**A. Eceiza, M. Larrañaga, K. de la Caba, G. Kortaberria, C. Marieta, M. A. Corcuera, I. Mondragon**

*Departamento Ingeniería Química y Medio Ambiente, Escuela Universitaria Politécnica, Universidad País Vasco/Euskal Herriko Unibertsitatea, Plaza Europa 1, 20018 Donostia-San Sebastián, Spain*

Received 15 February 2006; accepted 8 February 2007
DOI 10.1002/app.26553
Published online in Wiley InterScience (www.interscience.wiley.com).

**ABSTRACT:** The phase-separation behavior and morphology of polycarbonate-based polyurethanes were investigated as a function of the soft-segment molecular weight and chemical structure and the 4,4′-diphenylmethane diisocyanate/1,4-butanediol based hard-segment contents. Polarized optical microscopy and atomic force microscopy images showed that the surface morphologies changed as the soft-segment molecular weight and hard-segment content varied and also when the sample preparation conditions were modified. An increase in the soft- and hard-segment lengths led to increased phase separation with respect to the lower molecular weight soft segment, and this showed an interlocked and connected morphology of intermixed soft and hard domains. The surface morphology of phase-separated polyurethanes with hard segments composed of more than four to five 4,4′-diphenylmethane diisocyanate units contained globular hard-segment domains formed by spherulites, in which the size and connectivity between the branched lamellae changed with the hard-segment size. Interlamellar areas related to the soft segment were seen in the spherulites. Variations in the hard-segment spherulites were observed for polyurethanes based on soft segments of different molecular weights. © 2008 Wiley Periodicals, Inc. J Appl Polym Sci 108: 3092–3103, 2008

**Key words:** atomic force microscopy (AFM); microstructure; polyurethanes

## INTRODUCTION

Considerable attention has been devoted in recent years toward an understanding of the property–structure relationships in segmented polyurethanes.[1–3] These materials are usually randomly segmented copolymers of alternating flexible soft segments and more rigid, urethane-containing hard segments. In general, these materials derive their unusual elastomeric properties from the thermodynamic incompatibility of the polymer segments and their consequent microphase separation on a length scale comparable to the dimensions of the chain segments.

The mechanical properties of these materials are highly dependent on the degree of microphase separation.[1,4] This degree, however, not only is a function of the system thermodynamics but also depends on the ability of hard segments to pack correctly to form hydrogen bonds, and it is related to the chemical structure and composition of the copolymer.[5,6] Hard-segment packing is affected by some structural factors: the diisocyanate size and symmetry; the chain-extender length and functionality; and the polyol type, molecular weight, and functionality.[8–10] In addition, there is the distribution of hard-segment lengths, which is highly dependent on the stoichiometry and conversion of the condensation copolymerization.[11,12] The microphase-separation degree is also affected by the synthesis conditions, in bulk or in solution, with solvents of different polarities.[13] Finally, hard-segment packing is often a nonequilibrium process that depends on the thermal and mechanical history of a sample.[14–16] The understanding of these materials requires careful consideration of chemical and physical factors, opening a wide range of potential applications.

Microphase-separation and morphology studies of segmented polyurethane elastomers have been based mostly on small-angle X-ray scattering[8,9,11,17–25] and thermal characterization techniques.[8,9,15,20,22,26–28] Transmission electron microscopy (TEM) studies of stained films[24,29–31] have provided insight into the micromorphology of segmented polyurethanes. The experiments are limited by the inherent difficulties of sample preparation and/or the efficacy of staining, the possibility of beam damage, the low contrast between microdomains, and the possible misinterpretation of artifacts, so much of this work may be inconclusive. Morphologies containing spherical, cylindrical, or lamellar microdomains that depend on the

*Correspondence to:* I. Mondragon (inaki.mondragon@ehu.es).

Contract grant sponsor: Gipuzkoako Aldundia; contract grant number: 0207/2005.
Contract grant sponsor: Ministry of Education and Science of Spain; contract grant number: MAT2003-08125.
Contract grant sponsor: Basque Government (through Etortek 2005/BiomaGUNE 2005; contract grant number: IE05-143.

**TABLE I**
**Characteristics of the Different Materials**

| Chemical | Molecular weight (g/mol) | Glass-transition temperature (°C) | Melting temperature (°C) | State |
|---|---|---|---|---|
| 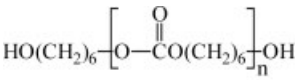 (PHMCD$_{1015}$) | 1015[a] | −74 | 48 | Solid |
| 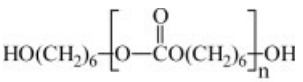 (PHMCD$_{1990}$) | 1990[a] | −64 | 53 | Solid |
| 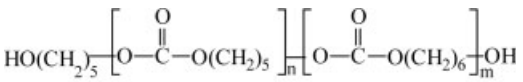 n = 5 and m = 7 (PHMPMCD) | 1850[a] | −63 | — | Liquid |
| 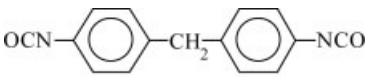 (MDI) | 250 | — | 38 | Solid |
| 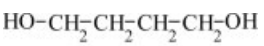 (BD) | 90 | — | 20 | Liquid |

[a] Determined by titration with ASTM D 4274-88 Test Method A.

chemical composition and hard-segment content have been reported.[32] More recently, atomic force microscopy (AFM), particularly tapping-mode AFM, has been proven to be an important tool for elucidating the microphase-separated structure of a variety of block copolymers,[33–38] including some polyurethanes.[4,33,39,40] Tapping-mode AFM has gained popularity for soft materials because of the low forces involved and because there is only intermittent contact between the sample and the tip in this mode, unlike the contact mode. This technique allows the simultaneous detection of height information and phase information, which provide insight into the variations of the topography and local stiffness, respectively. AFM has allowed the observation of dispersed, globular, and cylindrical or lathlike hard-segment-enriched microphases, and this is supported by TEM findings.

The aim of this study was to investigate the effect of the soft-segment structure and molecular weight and the ratio of the hard and soft components on both the phase separation and morphology of polycarbonate-based polyurethanes that could be used in a variety of biodegradable or biostable implantable medical devices. Because the phase separation and hard-segment/soft-segment domain structure depend on the sample preparation conditions, particularly for copolymers with high hard-segment contents,[41] the surface morphology and bulk morphology were investigated with AFM, polarized optical microscopy (POM), and differential scanning calorimetry (DSC).

## EXPERIMENTAL

### Materials and synthesis

Segmented polyurethanes of various hard-segment contents and of several soft-segment molecular weights and chemical structures were used in this study. The hard segment consisted of 4,4′-diphenylmethane diisocyanate (MDI), which was kindly supplied by Bayer (Leverkusen, Germany) under the trade name Desmodur 44, and 1,4-butanediol (BD) as a chain extender from Fluka (Steinheim, Germany). The soft segments were two polyhexamethylene carbonate diols, PHMCD$_{1015}$ and PHMCD$_{1990}$, with molecular weights of 1015 and 1990 g/mol, respectively, and a polyhexamethylene–pentamethylene carbonate diol (PHMPMCD) with a molecular weight of 1850 g/mol, which was kindly supplied by Polimeri Europa (Ravenna, Italy). The formulas, compositions, molecular

**TABLE II**
**Nomenclature of the Polyurethanes**

| Polymer | Macrodiol/MDI/ BD molar ratio | Hard segment (wt %) |
|---|---|---|
| $PHMCD_{1015}37$ | 1/2/1 | 37 |
| $PHMCD_{1015}60$ | 1/5/4 | 60 |
| $PHMCD_{1990}20$ | 1/1.8/0.8 | 20 |
| $PHMCD_{1990}30$ | 1/2.8/1.8 | 30 |
| $PHMCD_{1990}40$ | 1/4/3 | 40 |
| $PHMCD_{1990}50$ | 1/6/5 | 50 |
| $PHMCD_{1990}60$ | 1/9/8 | 60 |
| PHMPMCD40 | 1/4/3 | 40 |
| PHMPMCD59 | 1/8/7 | 59 |

weights, melting and glass-transition temperatures, and physical states at room temperature are listed in Table I.

Polyurethanes were prepared with a two-step bulk polymerization procedure. Before the reaction, all the polycarbonate diols were dried in a rotary evaporator under vacuum at 80°C for at least 24 h; BD and MDI were used as received. Dried polycarbonate diol and an excess of diisocyanate were placed in a three-necked, round-bottom flask. The flask was fitted with a dry nitrogen inlet, a condenser, and a mechanical stirrer and was heated in a thermoregulated silicon bath at 80°C. According to kinetic measurements previously reported,[42] the mixture was kept stirring for 2 h to endcap the macrodiol with isocyanate. BD was added to the prepolymer at 60°C with rapid stirring with a stainless steel paddle for 2 min to homogenize the mixture and to evacuate the air trapped within. The resulting viscous liquid was quickly poured between two Teflon-coated metal plaques separated by 2 mm and left to cure under pressure for 12 h at 100°C. The code for the compression-molded samples is expressed as macrodiol nameXX, where XX denotes the hard-segment content. For instance, the polyurethane prepared from $PHMCD_{1990}$ with a hard-segment content (MDI and BD) of 40 wt % was designated $PHMCD_{1990}40$. Table II lists the nomenclature, the molar ratios of the macrodiol, diisocyanate, and chain extender employed, and the hard-segment contents expressed as weight fractions of the hard segment (wt %) used in this work. The resulting polymers were strong, high-modulus elastomers that ranged from translucence to near opacity as the hard-segment content increased.

## Characterization techniques

### DSC

DSC thermograms were created in a Mettler–Toledo DSC822e apparatus calibrated with indium and equipped with an intracooler system. The thermal behavior was investigated through the scanning of the samples from −60 to 255°C or from 25 to 240°C under a dry nitrogen atmosphere at a scan rate of 20°C/min. The sample weights were 7–10 mg.

The midpoint of the heat capacity change was chosen to represent the glass-transition temperature, and the melting point refers to the endotherm peak temperature.

### Optical microscopy

The long-range supermolecular morphology was characterized by optical microscopy of a 100-μm microtomed film compressed between clean glass coverslips and of the prepared free surface of a sample of a 200-μm microtomed film placed on a glass cover. In both experiments, the samples were melted at 250°C and left to reach room temperature by cooling very slowly inside an oven. The cooling rate was calculated from the slope of the temperature profile. The cooling rate changed from 2.7°C/min at the beginning to 0.075°C/min at the end, and the entire cooling process lasted 550 min.

Many authors have suggested that the urethane group is unstable at high temperatures and that, depending on the type of diisocyanate, the structure of the hard segment, and the composition of the polyurethane, thermal degradation reactions can occur during cooling from the melt.[43,44] The changes have been explained by molecular rearrangements and variations in the crystalline structure. Two mechanisms of rearrangement have been discussed, depending on the hard-segment structure and the thermal treatment temperature: a thermal dissociation of the urethane bond, that is, a reurethanization or transurethanization, which is indicated by the free isocyanate, and an exchange of urethane groups between adjacent chains via a four-center-type reaction. To check the thermal stability, several experiments with samples obtained from bulk polymerization and also samples melted and subsequently cooled very slowly from the melt were performed. The molecular weights and molecular weight distributions were analyzed by size exclusion chromatography with a PerkinElmer chromatograph equipped with a binary pump and a refractive-index detector. The mobile phase was tetrahydrofuran (THF), and the separation was carried out with three Styragel columns packed with 5-μm particle gel with nominal pore sizes of 100, 500, and $10^4$ Å with an elution rate of 1 mL/min at 30°C. The samples were dissolved to 1 wt % in THF. The molecular weights and molecular weight distributions were based on a calibration curve with monodisperse polystyrene standards. The formation or disruption of different bonds between atoms in several functional groups was followed with Fourier transform infrared (FTIR) spectroscopy with a Nicolet Nexus FTIR spectrometer. The samples were dissolved in THF and were cast over KBr windows. After the THF evaporation, spectra of the

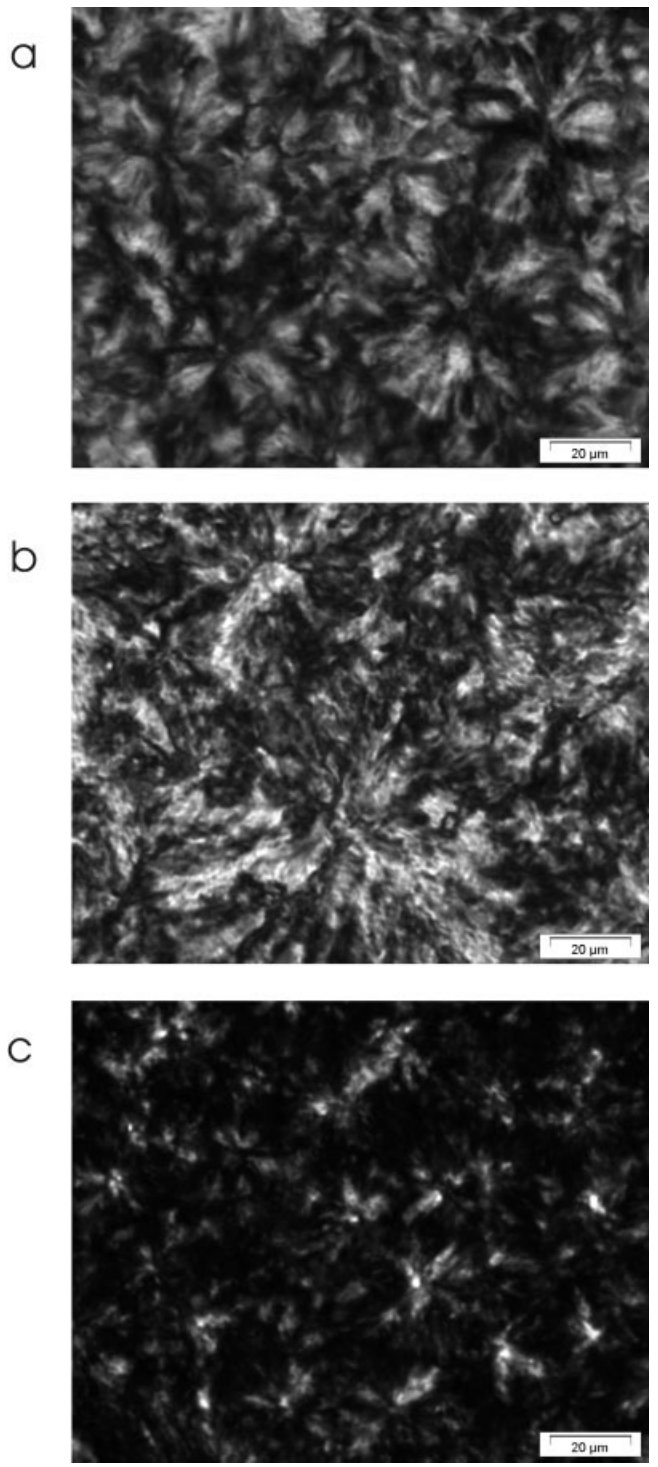


**Figure 1** Polarized optical micrographs of 100-μm microtomed film melt samples compressed between clean glass coverslips at 250°C and left to reach room temperature by cooling very slowly inside an oven: (a) $PHMCD_{1015}60$, (b) PHMPMCD59, and (c) PHMPMCD40.

samples were obtained from an average of 40 scans between 4000 and 400 $cm^{-1}$ with a resolution of 2 $cm^{-1}$. The weight loss was analyzed by thermogravimetric analysis (TGA) with a Setaram 92-12 apparatus in a dry helium atmosphere. The samples were heated from 30 to 900°C at a heating rate of 20°C/min. No variations were observed in the molecular weight or molecular weight distribution in the FTIR spectra. By TGA, the weight loss was not observed until 270°C, that is, above the temperature range employed for the sample preparation. Indeed, as no evidence of urethane group instability was observed in our samples after the thermal treatment, the experimental results were discussed under the assumption that no transurethanization or other thermal degradation reactions took place.

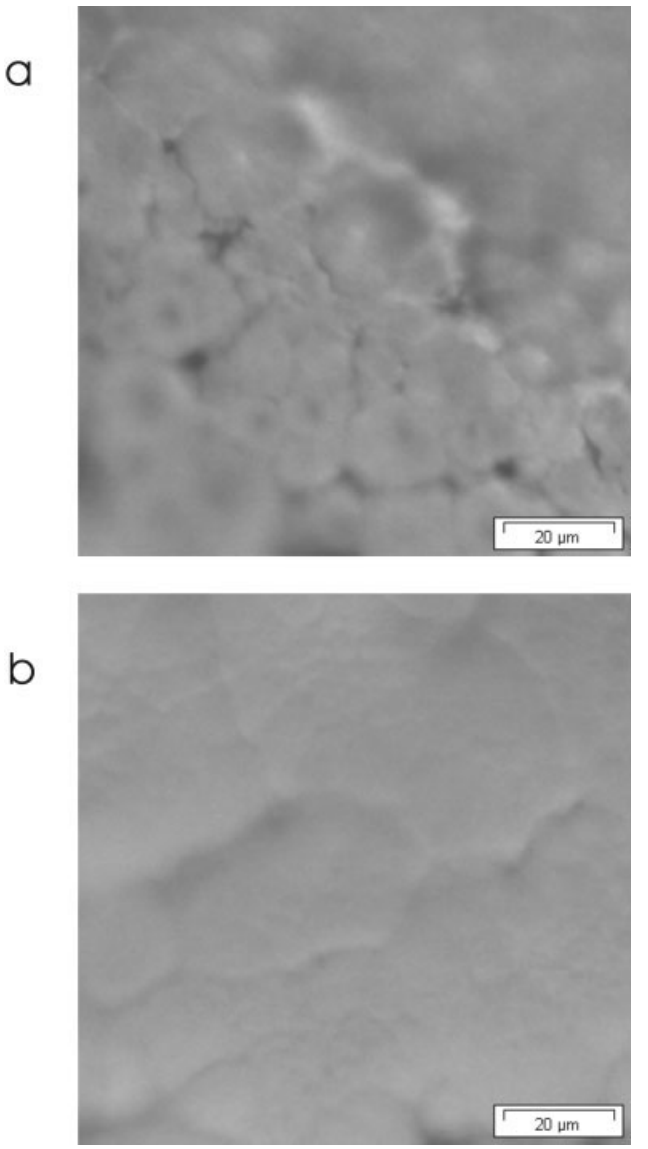


**Figure 2** Polarized optical micrographs of 200-μm microtomed film samples placed on glass covers, melted at 250°C, and left to reach room temperature by cooling very slowly inside an oven: (a) $PHMCD_{1015}60$ and (b) PHMPMCD59.

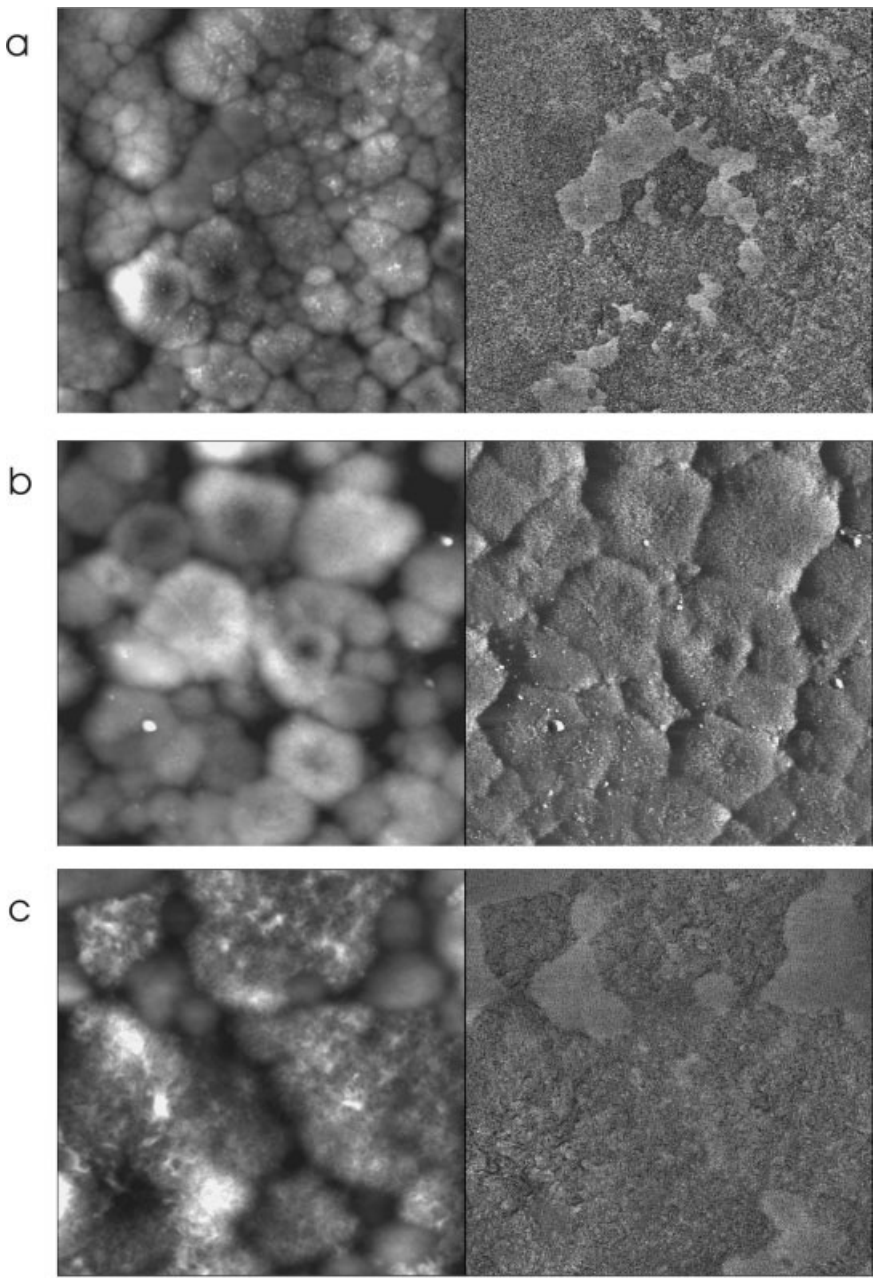


**Figure 3** AFM tapping-mode images of free surfaces as a function of the soft-segment molecular weight: (a) PHMPMCD59 (50 × 50 $\mu m^2$; height scale = 0–812 nm; phase scale = 0–50°), (b) $PHMCD_{1015}60$ (15 × 15 $\mu m^2$; height scale = 0–353 nm; phase scale = 0–54°), and (c) PHMPMCD59 (15 × 15 $\mu m^2$; height scale = 0–442 nm; phase scale = 0–48°).

Micrographs were obtained between crossed polarizers at room temperature with a Nikon Eclipse E600 light microscope equipped with a digital camera.

## AFM

Tapping-mode AFM was used to obtain height and phase image data simultaneously on a Nanoscope IIIa atomic force microscope from Digital Instruments. Silicon probes were used with a nominal constant of 20–100 N/m with 125-μm-long cantilevers at their fundamental resonance frequencies, which typically varied between 200 and 400 kHz. The cantilevers had a very small tip radius of 5–10 nm. The level of the force applied to the surface affected the phase data. These forces were roughly adjusted by the ratio of the set-point amplitude to the free-vibration amplitude in air. The set-point amplitude, which was used in feedback control, was adjusted to 40–70% of the free amplitude for moderate-force image mode data. Under these moderate-force tapping conditions, the phase data were sensitive to local stiffness differences of domains several nanometers from the uppermost

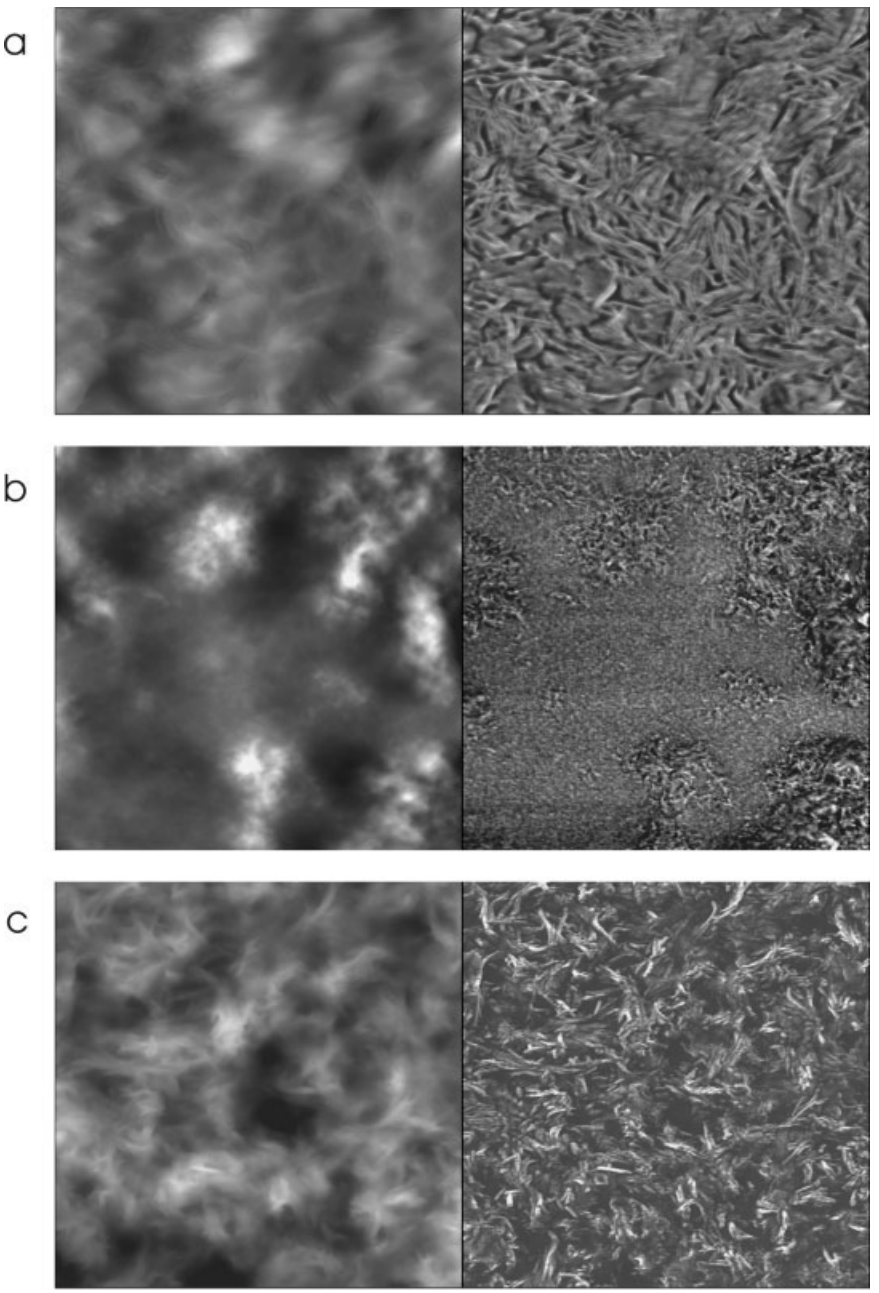


**Figure 4** AFM tapping-mode images of the free surfaces of (a) PHMPMCD59 ($2 \times 2$ μm$^2$; height scale = 0–112 nm; phase scale = 0–108°), (b) PHMCD$_{1015}$60 ($5 \times 5$ μm$^2$; height scale = 0–118 nm; phase scale = 0–36°), and (c) PHMCD$_{1990}$60 ($5 \times 5$ μm$^2$; height scale = 0–435 nm; phase scale = 0–59°).

surface. The soft segments were anticipated to give dark contrast in the phase imaging, whereas the hard segments appeared as bright areas,[30,33,45,46] provided that the phase-angle differences due to adhesion contrast or hydrophilicity of the surfaces did not have significant effects, and local stiffness seemed to govern the results.

The free-surface morphology was evaluated for the same samples used in the optical microscopy measurements; they were mounted directly onto AFM sample steel disks with double-sided adhesive tape without any additional preparation. The bulk morphology was evaluated through the imaging of cross sections prepared by freeze-fracturing of the compression-molded samples at the temperature of liquid nitrogen.

## RESULTS AND DISCUSSION

The surface morphologies of the polyurethanes were analyzed with AFM in the tapping mode and POM.

Because at low cooling rates the hard segment crystallized, samples melted at 250°C and left to reach room temperature by cooling very slowly in the oven were used. Figure 1(a–c) shows the polarized micrographs of 100-μm microtomed films melt-compressed between clean glass coverslips. Negatively birefringent spherulites, the molecules oriented perpendicularly to the long axis of the fibrillar crystal, and radial lamellae, which exhibited clear Maltese cross patterns,[47–49] covering almost the entire area can be observed in the POM images. Hard-segment crystals were present in large quantities; they touched one another in samples PHMPMCD59 and $PHMCD_{1015}60$, which had similar hard-segment contents (60 wt %), but this occurred only to a lesser extent for PHMPMCD40 with a hard-segment content of 40 wt %. The biggest hard-segment spherulites in the PHMPMCD59 sample could be due to the fact that the hard segments contained more MDI units, eight, versus the five and four MDI units in $PHMCD_{1015}60$ and PHMPMCD40, respectively. Therefore, it was possible to distinguish the fine anisotropic structure with a characteristic dendritic-like structure. The surfaces of $PHMCD_{1015}60$ and PHMPMCD59 prepared from microtomed film samples of 200 μm placed on a glass cover were also observed [Fig. 2(a,b)]. No negative spherulites with the distinct feature of a Maltese cross were visible under polarized light as separate elements. The surface contained numerous individual spherical or globular hard-segment domains, which could be composed of a superposition of spherulites growing in different directions or lamellae growing within the spherulites in different directions to the radial axis of the spherulites.[50] Because of the larger thickness of the polyurethane sample, extensive crystal nucleation or branching of lamellae occurred in all directions. The transverse orientation of the lamellae in the spherulites may have affected the overall sign of the spherulite birefringence and might even have conferred a positive character if the population of the lamellae transverse to the radial axis of the spherulite had been profuse.[50] The hard-segment globular domains were between 12 and 24 μm in $PHMCD_{1015}60$ and between 22 and 50 μm in PHMPMCD59. The hard-segment globular domains seemed to be formed of smaller domains or positive spherulites crowded together in bigger globular domains. Figure 3(a–c) shows AFM micrographs of the same samples. Now, it was possible to distinguish that the hard-segment globular clusters were composed of the aforementioned positive spherulites [Fig. 3(a,b)]. The measured size ranges of the hard-segment spherulites were between 2 and 4 μm and between 4 and 7 μm for $PHMCD_{1015}60$ and PHMPMCD59, respectively, according to their different hard-segment chain lengths. The spherulites showed a radial structure consisting of branched lamellae, that is, a spherulitic superstructure [Fig. 3(b,c)].

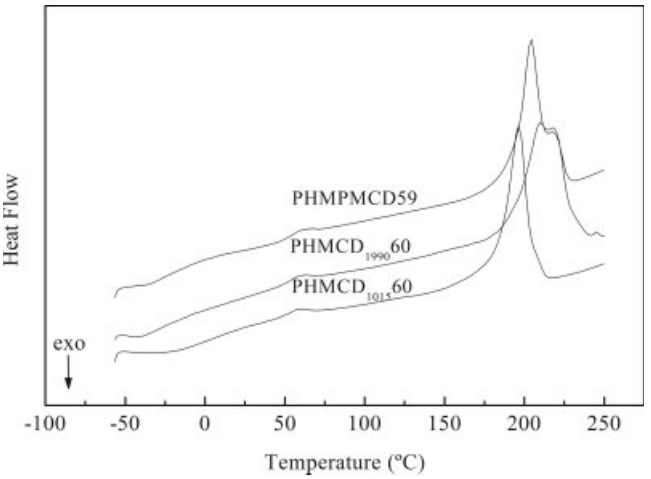


**Figure 5** DSC thermograms of $PHMCD_{1015}60$, $PHMCD_{1990}60$, and PHMPMCD59 free-surface polyurethane samples used to obtain AFM images.

The size of the lamellae, the level of hard-domain connectivity in them, and the intraspherulitic details are shown in the AFM images obtained at a higher magnification [Fig. 4(a–c)]. The surface of PHMPMCD59 was formed by an interconnected lamellar structure with lamellae about 500 nm long. Between the lamellae, dark areas were present, which could be attributed to the interlamellar soft segment. The radiating structural elements observed within the spherulites could be assigned to the hard segment. For $PHMCD_{1015}60$, because the hard segment was composed of five MDI units, the spherulites were composed of smaller lamellae, about 100 nm, and the entire surface was not covered with these lamellae. Very short hard-segment domains that phase-separated on the nanometer scale and were embedded in the soft-segment matrix could be seen around the spherulites for $PHMCD_{1990}60$. The surface was covered with hard-segment lamellae with sizes similar to those observed in PHMPMCD59. This fact could be explained if we take into account that, as the hard-segment length increased and/or the soft-segment molecular weight increased, the degree of phase separation increased, and more developed hard-segment structures were formed. Despite the similar soft-segment molecular weights and the same hard-segment content for $PHMCD_{1990}60$ and PHMPMCD59, different lamellar packing densities were observed, probably because of the different structures of the soft segments. The higher packing density observed in the PHMPMCD59 polyurethane could be explained by its higher tendency to form intramolecular hydrogen bonds with an odd number of methylene groups in the soft segment.[51]

Figure 5 shows the DSC thermograms of the samples used to obtain the AFM images. They confirm

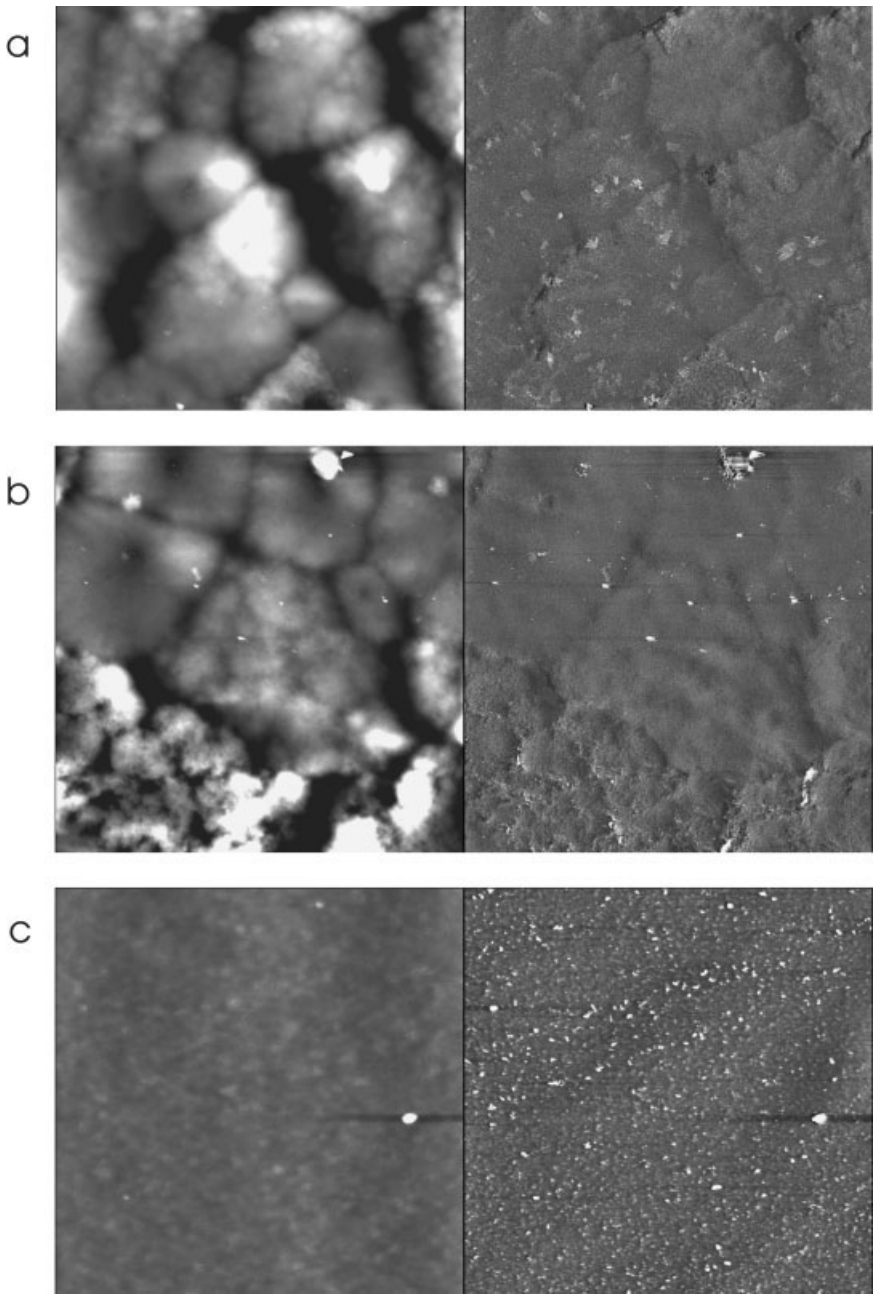


**Figure 6** AFM tapping-mode images of the free surfaces of (a) $PHMCD_{1990}40$ (30 × 30 μm$^2$; height scale = 0–537 nm; phase scale = 0–65°), (b) PHMPMCD40 (30 × 30 μm$^2$; height scale = 0–289 nm; phase scale = 0–55°), and (c) $PHMCD_{1015}37$ (5 × 5 μm$^2$; height scale = 0–28 nm; phase scale = 0–65°).

the existence of different crystalline aggregates. The endotherm observed at 197°C in $PHMCD_{1015}60$ was associated with the melting of spherulites formed of small lamellae, as observed by AFM, whereas the endotherms observed in $PHMCD_{1990}60$ and PHMPMCD59 in the range of 205–220°C could be due to the melting of spherulites formed of larger lamellae. Two melting peaks were observed for $PHMCD_{1990}60$ and PHMPMCD59, possibly because of different structures or lamellar sizes not revealed by AFM. The melting temperatures of $PHMCD_{1990}60$ were slightly higher than those for PHMPMCD59. It must be highlighted that one more MDI unit was included in the spherulites of $PHMCD_{1990}60$, affecting the packing level of the hard segment. The transition observed between 50 and 60°C was attributed to some relaxation effects of the polymer chain in the hard-segment phase due to the physical aging.[52] The DSC melting peek assignation was performed on the basis of the theoretical MDI–BD units in the hard segment and the different structures observed in the POM and AFM images.

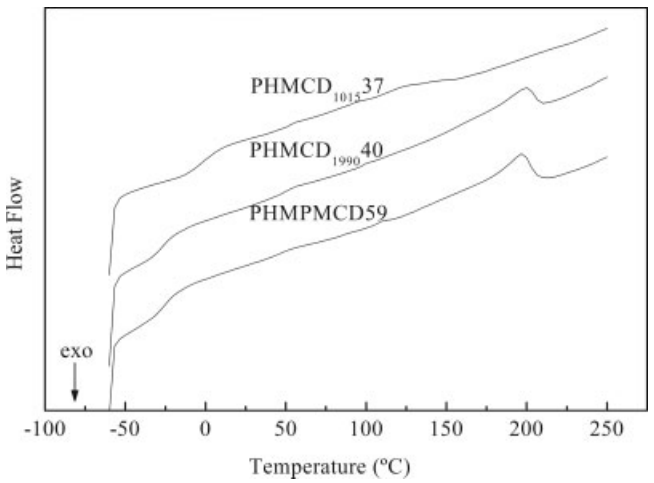


**Figure 7** DSC thermograms of $PHMCD_{1015}37$, $PHMCD_{1990}40$, and PHMPMCD40 free-surface polyurethane samples used to obtain AFM images.

Because hard- and soft-segment lengths affect polyurethane phase separation, it becomes interesting to investigate the morphologies of the same polyurethane systems with lower hard-segment contents. Figure 6(a–c) shows the topographic and phase images for samples having similar hard-segment contents but different soft-segment molecular weights and chemical structures. The morphologies observed for both $PHMCD_{1990}40$ and PHMPMCD40 were very similar to those observed for $PHMCD_{1015}60$. The molar compositions of these three polyurethanes were similar; the hard segments were composed of four to five MDI units, and spherulites were observed for all of them. However, the spherulites of $PHMCD_{1990}40$ and PHMPMCD40 were bigger, with an average size between 4 and 6 μm, than those observed for $PHMCD_{1015}60$. This fact could be due to the higher tendency to separate into microphases of $PHMCD_{1990}40$ and PHMPMCD40 polyurethanes composed of a soft segment of a higher molecular weight and therefore the higher capacity of the hard segment to crystallize. Despite the higher magnification of the

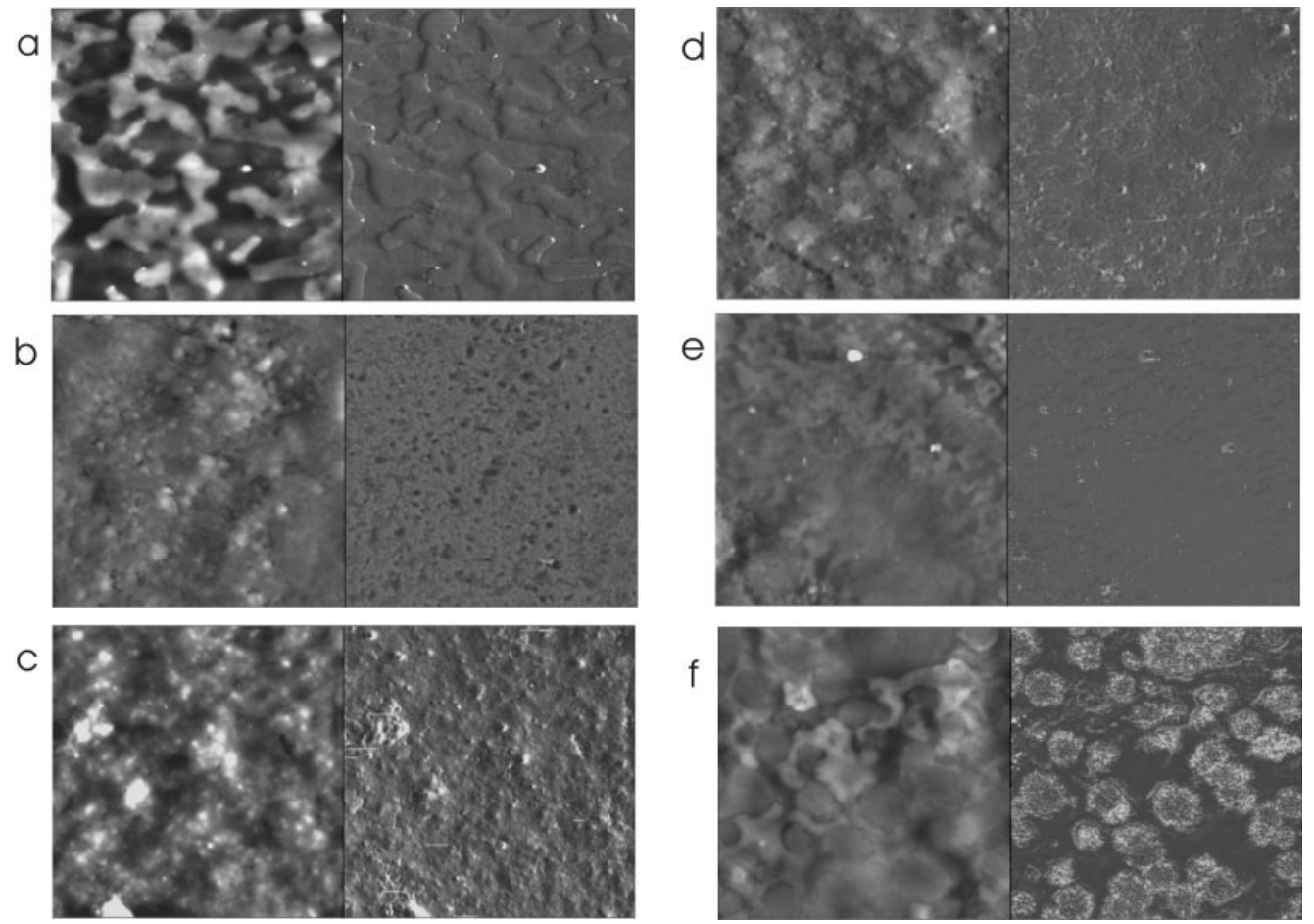


**Figure 8** AFM tapping-mode images of freeze-fractured cross sections as a function of the hard-segment content and soft-segment molecular weight: (a) $PHMCD_{1015}37$ (height scale = 0–267 nm; phase scale = 0–57°), (b) $PHMCD_{1015}60$ (height scale = 0–520 nm; phase scale = 0–58°), (c) $PHMCD_{1990}40$ (height scale = 0–155 nm; phase scale = 0–37°), (d) $PHMCD_{1990}60$ (height scale = 0–147 nm; phase scale = 0–28°), (e) PHMPMCD40 (height scale = 0–317 nm; phase scale = 0–135°), and (f) PHMPMCD59 (height scale = 0–508 nm; phase scale = 0–180°). The images are 20 × 20 $\mu m^2$.

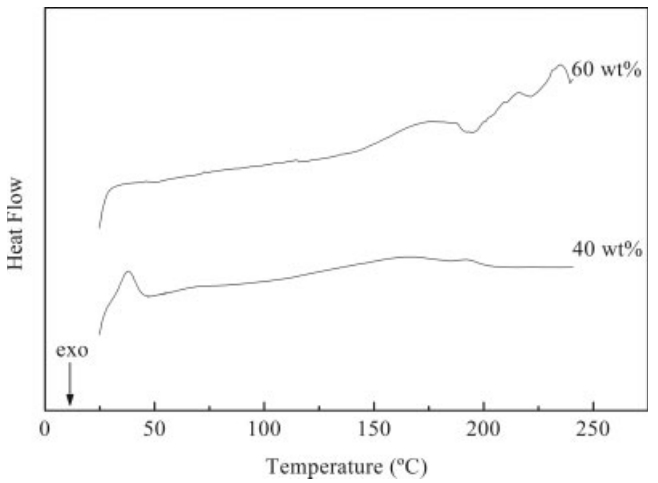


**Figure 9** DSC thermograms of $PHMCD_{1990}40$ and $PHMCD_{1990}60$ polyurethane samples.

$PHMCD_{1015}37$ polyurethane image, no lamellar structure domains were observed, and an almost uniform surface covered with very short hard-segment structures embedded in the soft-segment matrix could be seen. First, the low molecular weight of the soft segment and, second, the few units of MDI in the hard segments reduced the degree of phase separation between the segments and the tendency of the hard segment to crystallize, despite the low cooling rates employed. Figure 7 shows DSC thermograms of $PHMCD_{1015}37$, $PHMCD_{1990}40$, and PHMPMCD40. In thermograms of $PHMCD_{1990}40$ and PHMPMCD40, three different features can be observed: melting endotherms associated with hard-segment spherulites, observed by AFM, at 199 and 197°C, respectively; a hard-segment relaxation enthalpy induced by physical aging at 50–60°C; and the soft-domain glass-transition temperature at −35°C. In the thermogram of $PHMCD_{1015}37$, no melting endotherm associated with hard-segment microcrystalline domains can be observed; however, two melting peaks at 124 and 145°C, attributed to the very short hard-segment domains, can be observed, and a glass-transition temperature at −2.7°C, close to the single-phase, two-component system,[53] confirms the higher degree of miscibility of the hard and soft segments. Hard segments composed of two MDI units did not form spherulitic phase-separated domains; they appeared to be dissolved in the soft-segment matrix.[20,54]

In addition to free surfaces, freeze-fractured cross sections were analyzed to investigate the bulk morphology. A series of these images is shown in Figure 8(a–f). Figure 8(a,b) shows 20-μm-scan-size images of polyurethanes based on $PHMCD_{1015}$ with hard-segment contents of 37 and 60 wt %, respectively. The topographic and phase images of $PHMCD_{1015}37$ show an almost uniform surface covered by an interlocked and connected morphology developed from intermixed soft and hard domains. In the image of the $PHMCD_{1015}60$ polyurethane, an interlocked morphology of smaller domains can be observed. Therefore, the sample preparation condition affects the phase separation of segments and consequently a polyurethane's morphology. This fact can be very important in processes in which surface interactions are involved.

Figure 8(c,d) shows the morphology of polyurethanes based on $PHMCD_{1990}$ with hard-segment concentrations of 40 and 60 wt %, respectively. The morphology of the $PHMCD_{1990}40$ polyurethane was relatively uniform, being formed of small, irregular structures densely packed and evenly distributed throughout the polymer surface. The association of these structures can be seen in the microscale regions, which are irregular in shape and size and are highly interconnected. At higher hard-segment contents, in $PHMCD_{1990}60$, well-separated globular structures were observed. They seemed to be nearly identical in appearance and similar in size, typically 2 μm; however, smaller structures of 400 nm were also seen. Figure 9 shows the DSC thermograms of $PHMCD_{1990}40$ and $PHMCD_{1990}60$. The melting temperatures measured for the $PHMCD_{1990}40$ hard-segment structures are 163 and 193°C, and they have been attributed to different long-range-ordered structures.[19,20] The melting temperature of 215°C, measured for the $PHMCD_{1990}60$ polyurethane, has been attributed to the melting of 2-μm globular structures, and the melting temperature of 173°C has been attributed to the smaller, long-range-ordered structures. As the hard-segment content increased, the degree of phase separation increased, and more developed hard-segment structures were formed.

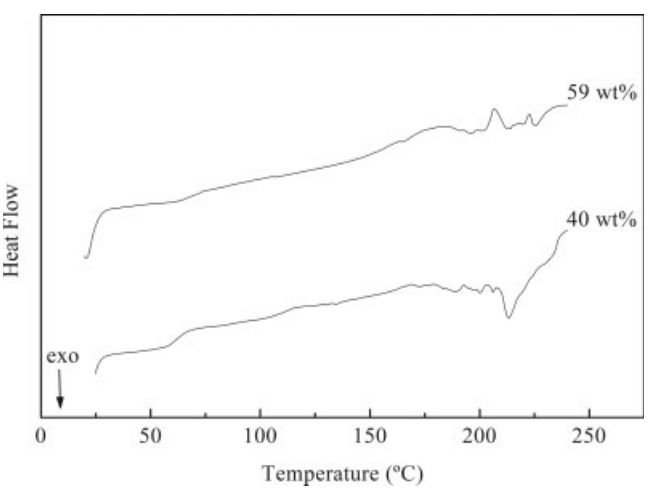


**Figure 10** DSC thermograms of PHMPMCD40 and PHMPMCD59 polyurethane samples.

Figure 8(e,f) shows the morphology of polyurethanes based on PHMPMCD with hard-segment concentrations of 40 and 59 wt %. As the hard-segment content increased, the hard-segment chains became longer and included more MDI/BD units. PHMPMCD59 contained numerous spherical and almost regular globular domains with an average size of 2–3 μm and even lamellar structures attributed to the hard segment. In PHMPMCD40, no formation of individual globular domains could be seen; the entire surface was covered with irregular hard-segment domains embedded in the soft-segment matrix. Figure 10 shows the DSC thermograms of PHMPM40 and PHMPMCD59 polyurethanes. Endotherms associated with long-range-ordered structures were observed for both polyurethanes at 120 and 180°C, respectively. The endotherm at 207°C observed in the DSC thermogram for PHMPMCD59 was associated with the melting of the microcrystalline hard-segment structures observed by AFM. As observed on the basis of the melting endotherm, the individual hard-segment structures observed in $PHMCD_{1990}60$ and PHMPMCD59, with hard segments of eight or nine MDI units, were able to form continuous microcrystalline hard microdomains, and they provided, because of physical crosslinks, structural reinforcement.

As shown previously, different crystalline structures are observed between the free surface and bulk. A plausible explanation is that in the case of a free surface, the chain segments of polyurethane have the ability to fully reorient or rearrange during cooling from an elevated temperature. This allows hard segments to aggregate to form dense hard-segment domains in which a relatively perfect crystalline region develops. Higher and narrower melting temperatures have been observed for these structures. On the contrary, a less perfect crystalline structure of the cross section of compression-molded samples might be formed because the hard segments and soft segments do not fully separate at the lower temperature used in the preparation of these samples; therefore, some of the soft segments would be dragged into the hard-segment domains, and this would limit the crystallization of hard segments.

It has also been shown that the composition of a polymer surface depends on the chemical structure and molecular weight of the soft segment, on the hard-segment content, and on the preparation conditions. The successful application of polycarbonate-based polyurethanes in the field of medicine depends on their biocompatibility and biostability. It is accepted that the interactions between biological systems responsible for degradation and artificial surfaces occur at the tissue–biomaterial interface. Therefore, it is reasonable to expect that the nature of the surface will influence these interactions.

## CONCLUSIONS

The phase separation, structure, and morphology of polycarbonate-based thermoplastic polyurethanes have been investigated as a function of the soft-segment structure and molecular weight and with the variation of their hard-segment content with mainly POM and AFM. The effect of the sample preparation conditions has also been investigated. As the soft-segment molecular weight increases and at elevated hard-segment contents, AFM images show a phase-separated morphology with the formation of hard-segment globular domains, which is higher as the hard-segment content increases. The intensity and position of high melting temperatures observed in polyurethanes are affected by phase separation between segments, being dependent on the hard-segment content, that is, the stoichiometry. The availability to form hydrogen bonds between hard segments increases with an increase in the number of MDI–BD units, and thus the capability to crystallize does as well. Therefore, the melting peak moves to higher temperatures. Phase-separated, high-melting-temperature hard-segment microdomains provide physical reinforcements able to impart elastomeric properties over a wide range of temperatures and enhance the thermal stability of polyurethanes. Because the biocompatibility and surface-initiated biodegradation response of these thermoplastic polyurethanes depend strongly on the morphology, mainly on the surface morphology, the success of this type of polycarbonate-based polyurethane in biomedical applications will depend on the chemistry and molecular weight of the soft segment and also on the hard-segment content, which controls its morphology.

## References

1. Adhikari, R.; Gunatillake, P. A.; McCarthy, S. J.; Meijs, G. F. J Appl Polym Sci 2000, 78, 1071.
2. Saiani, A.; Daunch, W. A.; Verbeke, H.; Leenslag, J. W.; Higgins, J. S. Macromolecules 2001, 34, 9059.
3. Saiani, A.; Rochas, C.; Eeckhaut, G.; Daunch, W. A.; Leenslag, J. W.; Higgins, J. S. Macromolecules 2004, 37, 1411.
4. Kim, Y. S.; Lee, J. S.; Ji, Q.; McGrath, J. E. Polymer 2002, 43, 7161.
5. Bonart, R.; Morbitzer, L.; Muller, E. H. J Macromol Sci Phys 1974, 9, 447.
6. Wilkes, G. L.; Emerson, J. A. J Appl Phys 1976, 47, 4261.
7. Leung, L. M.; Koberstein, J. T. Macromolecules 1986, 19, 706.
8. Velankar, S.; Cooper, S. L. Macromolecules 1998, 31, 9181.
9. Velankar, S.; Cooper, S. L. Macromolecules 2000, 33, 382.
10. Sheth, P. J.; Aneja, A.; Wilkes, G. J.; Yilgor, E.; Atilla, G. E.; Yilgor, I.; Beyer, F. L. Polymer 2004, 45, 6919.
11. Speckhard, T. A.; Gibson, P. E.; Cooper, S. L.; Chang, V. S. C.; Kennedy, J. P. Polymer 1985, 26, 55.
12. Martin, D. J.; Meijs, G. F.; Renwick, G. M.; McCarthy, S. J.; Gunatillake, P. A. J Appl Polym Sci 1996, 62, 1377.
13. Boiteux, G.; Cuvé, L.; Pascault, J. P. Polymer 1994, 35, 173.
14. Kim, B. K.; Shin, Y. J.; Cho, S. M.; Jeong, H. M. J Polym Sci Part B: Polym Phys 2000, 38, 2652.

15. Hu, W, Koberstein, J. T. J Polym Sci Part B: Polym Phys 1994, 32, 437.
16. Chen, T. K.; Shied, T. S.; Chui, J. Y. Macromolecules 1998, 31, 1312.
17. Ophir, Z.; Wilkes, G. L. J Polym Sci Polym Phys Ed 1980, 18, 1469.
18. Van Bogart, J. W. C.; Gibson, P. E.; Cooper, S. L. J Polym Sci Polym Phys Ed 1983, 21, 65.
19. Leung, L. M.; Koberstein, J. T. J Polym Sci Polym Phys Ed 1985, 23, 1883.
20. Koberstein, J. T.; Russell, T. P. Macromolecules 1986, 19, 714.
21. Li, C.; Cooper, S. L. Polymer 1990, 31, 3.
22. Koberstein, J. T.; Galambos, A. F.; Leung, L. M. Macromolecules 1992, 25, 6195.
23. Laity, P. R.; Taylor, J. E.; Wong, S. S.; Khunkamchoo, P.; Norris, K.; Cable, M.; Andrews, G. T.; Johnson, A. F.; Cameron, R. E. Polymer 2004, 45, 5215.
24. Saiani, A.; Rochas, C.; Eeckhaut, G.; Daunch, W. A.; Leenslag, J. W.; Higgins, J. S. Macromolecules 2004, 37, 1411.
25. Sheth, J. P.; Aneja, A.; Wilkes, G. L.; Yilgor, E.; Atilla, G. E.; Yilgor, I.; Beyer, F. L. Polymer 2004, 45, 6919.
26. Hesketh, T. R.; Van Bogart, J. W. C.; Cooper, S. L. Polym Eng Sci 1980, 20, 190.
27. Van Bogart, J. W. C.; Bluemke, D. A.; Cooper, S. L. Polymer 1981, 22, 1428.
28. Chen, T. K.; Chui, J. Y.; Shieh, T. S. Macromolecules 1997, 30, 5068.
29. Schrader, S.; Li, X.; Guo, F.; Liu, Y.; Luo, J.; Xu, D. Makromol Chem Rapid Commun 1988, 9, 597.
30. Karbach, A.; Drechsler, D. Surf Interface Anal 1999, 27, 401.
31. Hamley, I. W.; Stanford, J. L.; Wilkinson, A. N.; Elwel, M. J.; Ryan, A. J. Polymer 2000, 41, 2569.
32. Laity, P. R.; Taylor, J. E.; Wong, S. S.; Khunkamchoo, P.; Norris, K.; Cable, M.; Chohan, V.; Andrews, G. T.; Johnson, A. F.; Cameron, R. E. J Macromol Sci Phys 2004, 43, 95.
33. McLean, R. S.; Sauer, B. B. Macromolecules 1997, 30, 8314.
34. Magonov, S. N.; Cleveland, J.; Elings, V.; Denley, D.; Whangbo, M.-H. Surf Sci 1997, 389, 201.
35. Motomatsu, M.; Mizutani, W.; Tokumoto, H. Polymer 1997, 38, 1779.
36. Pfau, A.; Janke, A.; Heckmann, W. Surf Interface Anal 1999, 27, 410.
37. Elbs, H.; Fukunaga, K.; Stadler, R.; Sauer, G.; Magerle, R.; Krausch, G. Macromolecules 1999, 32, 1204.
38. Serrano, E.; Martín, M. D.; Tercjak, A.; Pomposo, J. A.; Mecerreyes, D.; Mondragon, I. Macromol Rapid Commun 2005, 26, 982.
39. Tocha, E.; Janik, H.; Debowski, M.; Vancso, G. J. J Macromol Sci Phys 2002, 41, 1291.
40. Revenko, I.; Tang, Y.; Santerre, J. P. Surf Sci 2001, 491, 346.
41. Garrett, J. T.; Lin, J.; Runt, J. S. Macromolecules 2002, 35, 161.
42. Eceiza, A.; de la Caba, K.; Kortaberria, G.; Gabilondo, N.; Marieta, C.; Corcuera, M. A.; Mondragon, I. Eur Polym J 2005, 41, 3051.
43. Joel, D.; Hauser, A. Angew Makromol Chem 1994, 217, 191.
44. Steinlein, C.; Hernandez, L.; Eisenbach, C. D. Macromol Chem Phys 1996, 197, 3365.
45. O'Sickey, M. J.; Lawrey, B. D.; Wilkes, G. L. Polymer 2002, 43, 7399.
46. Aneja, A.; Wilkes, G. L. Polymer 2003, 44, 7221.
47. Briber, R. M.; Thomas, E. L. J Macromol Sci Phys 1983, 22, 509.
48. Takahashi, T.; Hayashi, N.; Hayashi, S. J Appl Polym Sci 1996, 60, 1061.
49. Furukawa, M.; Hamada, Y.; Kojio, K. J Polym Sci Part B: Polym Phys 2003, 41, 2355.
50. Hosier, I. L.; Alamo, R. G.; Lin, J. S. Polymer 2004, 45, 3441.
51. Eceiza, A.; de la Caba, K.; Gascón, V.; Corcuera, M. A.; Mondragon, I. Eur Polym J 2001, 37, 1685.
52. Chen, T. K.; Shieh, T. S.; Chui, J. Y. Macromolecules 1998, 31, 1312.
53. Fox, T. G. Bull Am Phys Soc 1956, 1, 23.
54. Koberstein, J. T.; Stein, R. S. J Polym Sci Polym Phys Ed 1983, 21, 1439.